ACS OMEGA

Open Access

http://pubs.acs.org/journal/acsodf

Article

BC_6N Monolayer as a Potential VOC Adsorbent in Mitigation of Environmental Pollution: A Theoretical Perspective

Xiaoshu Jiang and Xuan Luo*

Cite This: *ACS Omega* 2023, 8, 46841−46850

Read Online

ACCESS | Metrics & More | Article Recommendations

ABSTRACT: Rapid economic growth has led to severe air pollution, which poses threats to both the environment and public health. Among the major contributors to this issue are volatile organic compounds (VOCs), the abatement methods of which have received considerable attention from the research community. Recently, an adsorption technology employing two-dimensional monolayers has emerged as a promising strategy for VOC control. In the current investigation, we examined the adsorption behaviors of three prevalent VOCs, namely, acetone, benzene, and tetrachloromethane, on both pristine and Pd-doped BC_6N monolayers. Through first-principles calculations based on density functional theory, it was revealed that pristine BC_6N adsorbs acetone, benzene, and tetrachloromethane with modest adsorption energies of −0.003, −0.036, and −0.017 eV, respectively. These weak interactions make the adsorbate−adsorbent systems especially unstable, causing the VOCs to desorb from the pristine monolayer under increased ambient temperature or other environmental disturbances. The introduction of an interstitial Pd dopant has induced a significant improvement in the adsorption performance of the BC_6N monolayer. Specifically, the values of adsorption energy for acetone and benzene on the Pd-doped BC_6N monolayer experience a remarkable increase, measuring −0.745 and −1.028 eV, respectively. Moreover, the charge transfer is enhanced along with reduced adsorption distances, indicating strong chemisorption of acetone and benzene on the Pd-doped BC_6N monolayer. Our results establish the Pd-doped BC_6N monolayer as an efficient adsorbent for the toxic gases, particularly acetone and benzene, carrying practical implications for air quality improvement and environmental sustainability.

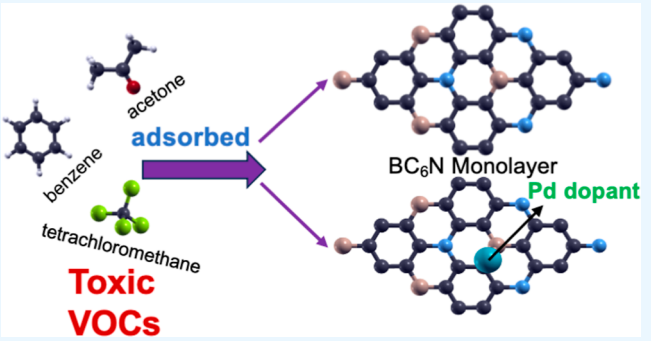

INTRODUCTION

The Canadian wildfires have stood out as one of the most prominent global environmental events in the year 2023.[1] By the end of July, over 121,000 km^2 of land have been burnt, resulting in severely damaged forest ecosystems.[2] Additionally, the wildfires have unleashed a massive influx of pollutants into the atmosphere, causing air quality to decrease swiftly. The condition posed a serious threat to the health of residents in Canada and the US East Coast.[3,4] Air pollution, as a major public health concern, has again come to the forefront of societal attention.[5,6] Based on statistics from the World Health Organization, approximately 7 million premature deaths every year can be attributed to air pollution. Airborne pollutants are commonly classified into gaseous pollutants, persistent organic pollutants, heavy metals, and particulate matter, which are all risk factors for respiratory and cardiovascular diseases.[7] Because of their roles in aggravating climate change, forming photochemical smog, and inducing acid rain,[8,9] gaseous pollutants, especially sulfur and nitrogen oxides (SO_2, NO, and NO_2), carbon monoxide (CO), and volatile organic compounds (VOCs), are identified as particularly hazardous. Recently, VOC pollution has received considerable attention from the research community due to their elevated concentrations in certain regions.[10,11]

VOCs are carbon-containing organic chemicals that have high vapor pressure under ambient conditions.[12] Both natural and anthropogenic activities release VOCs into the atmosphere, with the proportion of human-made VOCs steadily increasing.[11,13] While there exist over 300 types of ambient VOCs, they can generally be categorized into groups of aldehydes, aromatic compounds, polycyclic aromatic hydrocarbons, halogenated compounds, alcohols, and ketones.[14] When present at concentrations beyond the safe level, VOCs, especially ketones, aromatic compounds, and halogenated hydrocarbons, can produce profound adverse effects on human health and the ecological environment.[15−17] For instance,

Received: August 28, 2023
Revised: November 4, 2023
Accepted: November 10, 2023
Published: November 27, 2023

inhalation of high-concentration ketones like acetone can result in eye irritation and central nervous system depression.[14,18] Exposure to benzene, an aromatic compound, at dangerous levels poses fatal risks of leukemia and lymphomas.[19] Polychloromethanes such as tetrachloromethane are typical halogenated VOCs, which significantly contribute to global warming and ozone layer depletion by acting as radicals in the atmosphere.[20] Given their high toxicity, it is crucial to devise effective techniques for the removal of VOCs.

Efforts to control VOC emissions primarily involve recovery and destruction methods.[21] While some destruction methods like incineration and catalytic oxidation may necessitate rigorous maintenance and conditions, recovery methods, particularly adsorption technology, prove to be more efficient and economical.[13,22,23] Abundant research attests to the effectiveness of adsorbent materials like metal organic frameworks, activated carbon, biochar, and zeolites in adsorbing toxic environmental VOCs.[15,24] Recently, numerous two-dimensional (2D) monolayers have emerged as appealing candidates in environmental remediation applications due to their high surface-to-volume ratio, large number of active sites, and low cost.[25−29] Cao et al. have investigated the potential of the MnO_2 monolayer in adsorbing VOCs like formaldehyde and methyl chloride.[26] The silicon carbide monolayer was proposed by Yadav as adsorbents for benzene and other aromatic compounds.[27] It was also reported that Si-doped C_2N and Pt-doped graphene were suitable mediums for acetone removal.[28,29]

Among all the 2D materials, graphene has received the most attention in gas adsorption devices.[29,30] Nonetheless, the zero band gap greatly limits its application in toxic gas removal. To overcome this weakness, surface functionalization, defect engineering, and doping impurities are applied.[31,32] Particularly, substitutional doping of boron (B) and nitrogen (N) is proposed as a viable approach to open the band gap and improve the adsorption capability of graphene.[33,34] By replacing the carbon (C) atoms with the nearest neighbors of B and N atoms, graphene-like boron carbides (BC_3) and carbon nitrides (C_3N) are constructed, and their adsorption properties are also extensively studied.[35−38] Aghaei et al. have studied the adsorption of various toxic gases on the BC_3 monolayer and revealed the possibility of BC_3 as a catalyst for NO_2 dissociation.[35] The adsorption behaviors of acetone and other gases have also been investigated by Zhao et al., and they reported notable change in the optical properties of BC_3 after acetone adsorption.[36] Furthermore, the C_3N monolayer has been explored by Bafekry et al. as a promising adsorbent for NO, NO_2, and SO_2.[37] Pashangpour's study has shown the effectiveness of Al doping in improving the adsorption performance of C_3N toward CO.[38]

More excitingly, the BN-*co*-doped graphene borocarbonitride (BC_6N) was synthesized as a transitional structure between BC_3 and C_3N.[39] Engineered from graphene, BC_6N not only offers favorable physical properties including high carrier mobility and thermal conductivity but also exhibits semiconducting behavior.[40] Moreover, the acceptor and donor characteristics of B and N atoms offer BC_6N the potential in adsorbing a wide range of gases.[41] Yong et al. investigated the adsorption behaviors of NH_3 and showed that the adsorption could be enhanced by single vacancies and Stone−Wales defects in BC_6N.[42] It was also reported by Aasi et al. that introducing a transition metal dopant could effectively improve the adsorption performance of BC_6N toward inorganic gases such as SO_2, NO, and H_2S.[43] Aghaei et al. demonstrated significantly improved adsorption of various VOCs using single-vacancy-defected BC_6N.[44]

As BC_6N proves to be a tantalizing adsorbent, it was selected as the channel material for toxic VOC removal in the current research. Using first-principles calculations based on density functional theory (DFT), we investigated the adsorption performance of the BC_6N monolayer toward acetone, benzene, and tetrachloromethane. The three VOCs were chosen as they could represent categories of ketones, aromatic compounds, and halogenated compounds. To improve the limited adsorption capacity of pristine BC_6N toward VOCs, palladium (Pd), a transitional metal, was introduced into the monolayer. The structural properties and adsorption behaviors were analyzed and compared for both pristine and doped monolayers. Given the ubiquitous presence of VOCs in the ambient environment and the health risks they pose, it is worthwhile to search for potential high-performance material to mitigate their pollution. Through our theoretical research framework, we aim to answer the question of whether a Pd-doped BC_6N monolayer is a feasible candidate for efficient VOC capture.

METHOD

Computational Details. We performed first-principles calculations based on DFT employing the generalized gradient approximation with Perdew−Burke−Ernzerhof exchange−correlation functionals in the ABINIT package.[45,46] Pseudopotentials were generated by the projector augmented wave (PAW) implemented in the AtomPAW code.[47,48] The electron configurations and radius cutoffs of the elements used in the calculations are listed in Table 1.

Table 1. Electron Configurations and Radius Cutoffs (r_{cut}) of Elements Used for Generating Pseudopotentials

element	electron configuration	r_{cut} (Bohr)
hydrogen (H)	$1s^1$	1.0
boron (B)	$[He]2s^22p^1$	1.7
carbon (C)	$[He]2s^22p^2$	1.5
nitrogen (N)	$[He]2s^22p^3$	1.2
oxygen (O)	$[He]2s^22p^4$	1.4
chlorine (Cl)	$[Ne]3s^23p^5$	1.8
palladium (Pd)	$[Ar\ 3d^{10}]4s^24p^65s^14d^9$	2.5

For total energy calculations, the self-consistent force (SCF) iteration is terminated when the total energy difference is less than 1.0×10^{-10} Ha twice consecutively. Convergence with the kinetic energy cutoff, Monkhorst−Pack *k*-point grids, and vacuum was then carried on. The data set is said to be converged once the total energy difference is less than 0.0001 Ha (about 3 meV) twice consecutively, a reliable criterion used by most first-principles studies.[49−51] With the converged values, structural optimization calculations were conducted for VOCs adsorbed on the pristine and Pd-doped BC_6N monolayers. The tolerance for force differences of 5.0×10^{-5} Hartree/Bohr must be achieved twice to terminate the SCF iterations. The Broyden−Fletcher−Goldfarb−Shanno algorithm was employed for minimization,[52] with the maximal absolute force tolerance set to 1.0×10^{-3} Hartree/Bohr for stopping the molecular dynamics process.

Atomic Structures. The molecular configurations of acetone (C_3H_6O), benzene (C_6H_6), and tetrachloromethane

https://doi.org/10.1021/acsomega.3c06325
ACS Omega 2023, 8, 46841−46850

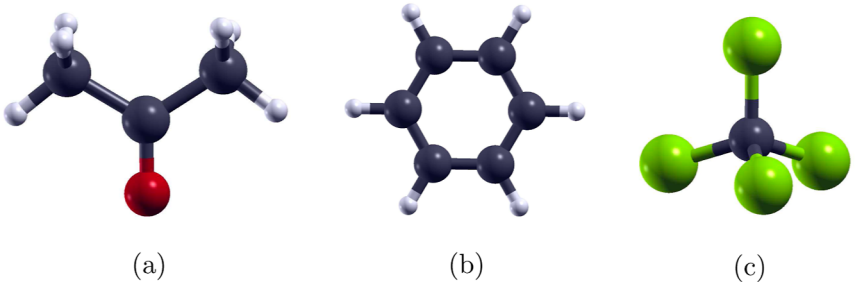

Figure 1. Atomic structures of VOC molecules. (a) Acetone (C_3H_6O). (b) Benzene (C_6H_6). (c) Tetrachloromethane (CCl_4). H, C, O, and Cl atoms are represented by white, gray, red, and green, respectively.

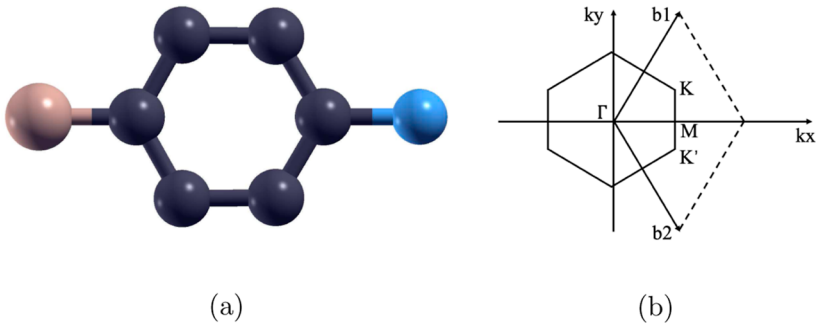

Figure 2. (a) Atomic structure of the 1 × 1 BC_6N monolayer. B, C, and N atoms are represented by pink, gray, and blue, respectively. (b) First Brillouin zone with high-symmetry *k*-points Γ, *M*, and *K*.

(CCl_4) were sourced from the Protein Data Bank and are presented in Figure 1. To optimize their atomic structures, relaxation calculations were conducted using a converged cell size.

Subsequently, we explored both pristine and doped monolayers for VOC adsorption. Figure 2a displays the 1 × 1 BC_6N monolayer, characterized by its graphene-like structure with B and N atoms substituting for two of the C atoms. For adsorption computations, the 1 × 1 BC_6N monolayer was expanded into a 2 × 2 supercell comprising 32 atoms, and the Pd-doped BC_6N monolayer was constructed by interstitially doping a Pd atom into the 2 × 2 BC_6N supercell. VOC molecules were then placed above both monolayers to analyze their adsorption behaviors.

Electronic Structure. To investigate the electronic properties, band structure calculations were performed for the pristine BC_6N monolayer, Pd-doped BC_6N monolayer, and VOCs−BC_6N complexes. High symmetry *k*-points in the first Brillouin zone Γ (0,0,0), *K* ($\frac{2}{3}$, $\frac{1}{3}$, 0), *M* ($\frac{1}{2}$, $\frac{1}{2}$, 0), and back to Γ (0, 0, 0) were used to generate the band structures, as shown in Figure 2b. To compare the differences in band structures, the percent change in the band gap (% ΔE_g) was further calculated using the following equation

$$\% \Delta E_g = \frac{E_g 2 - E_g 1}{E_g 1} \times 100 \quad (1)$$

where E_g1 and E_g2 are the energy band gaps (E_g) of the pristine or Pd-doped BC_6N monolayer before and after VOC adsorption, respectively.

We then calculated the charge transfer for the VOCs−BC_6N systems to have a better understanding of how BC_6N and Pd-doped BC_6N interact with VOCs during adsorption. The self-consistent energy calculations were performed separately to determine the separate charge densities of the VOC molecules, BC_6N monolayers, and the VOCs−BC_6N complexes in the same unit cell.

$$\Delta\rho(r) = \rho_{VOCs+ML}(r) - \rho_{ML}(r) - \rho_{VOCs}(r) \quad (2)$$

The equation above was used to determine the charge transfer [$\Delta\rho(r)$] for VOCs adsorbed on the BC_6N monolayer. $\rho_{VOCs+ML}(r)$ is the charge density of the VOCs−BC_6N adsorption systems. $\rho_{ML}(r)$ is the charge density of the pristine and Pd-doped BC_6N monolayers (ML). $\rho_{VOCs}(r)$ is the charge density of acetone, benzene, and tetrachloromethane. Charge depletion and charge accumulation are represented by negative and positive values of charge transfer, respectively. For better comparison, the values for plotting the charge transfer isosurface were kept the same for each VOC adsorbed on both pristine and Pd-doped BC_6N monolayers.

■ ENERGY CALCULATIONS

Defect Formation Energy. The defect formation energy (E_{form}) of the Pd-doped BC_6N monolayer was calculated using

$$E_{form} = E_{Pd-ML} - E_{ML} - E_{Pd} \quad (3)$$

where E_{Pd-ML}, E_{ML}, and E_{Pd} are the total energy of the Pd-doped BC_6N monolayer, total energy of the pristine BC_6N monolayer, and chemical potential of the Pd atom, respectively.

Adsorption Energy. Using the optimized structures, we performed total energy calculations for VOC molecules, pristine and Pd-doped BC_6N monolayers, and VOCs−BC_6N complexes. The adsorption energy for VOCs on the BC_6N monolayer was calculated by

$$E_{ad} = E_{VOCs+ML} - E_{ML} - E_{VOCs} \quad (4)$$

where E_{ad} represents the adsorption energy, $E_{VOCs+ML}$ represents the energy of BC_6N with VOCs adsorbed, E_{ML} represents the energy of pristine and Pd-doped BC_6N

https://doi.org/10.1021/acsomega.3c06325
ACS Omega 2023, 8, 46841−46850

Table 2. Bond Lengths (d) in Å and Bond Angles (θ) in Degrees (°) of Acetone (C_3H_6O), Benzene (C_6H_6), and Tetrachloromethane (CCl_4) from Past Experiments and Current Calculations

		d_{CH}	d_{CC}	d_{CO}	d_{CCl}	θ_{HCH}	θ_{HCC}	θ_{CCC}	θ_{CCO}	θ_{ClCCl}
C_3H_6O	current	1.10	1.51	1.22		106.5°	110.9°	116.6°	121.7°	
	experiment[53]	1.10	1.52	1.21		108.4°	110.5°	116.0°	122.0°	
C_6H_6	current	1.09	1.40				120.0°	120.0°		
	experiment[53]	1.08	1.40				120.0°	120.0°		
CCl_4	current				1.78					109.5°
	experiment[53]				1.77					109.5°

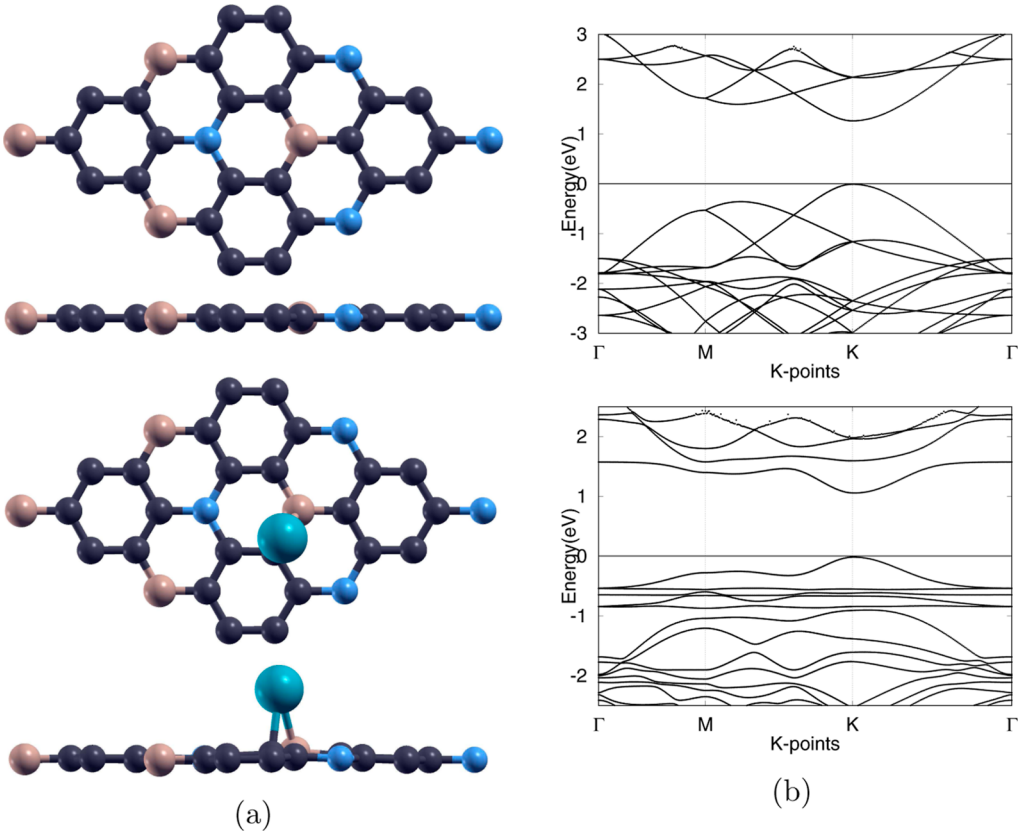

Figure 3. Atomic and electronic structures of pristine 2 × 2 BC_6N and Pd-doped BC_6N monolayers. (a) Top and side views of the optimized atomic structure of pristine (first row) and Pd-doped BC_6N (second row) monolayers. B, C, N, and Pd atoms are represented by pink, gray, blue, and cyan, respectively. (b) Band structures of pristine (first row) and Pd-doped (second row) BC_6N monolayers with the Fermi level set at zero. The conduction band minimum (CBM) and the valence band maximum (VBM) are located at the K point.

monolayers, and E_{VOCs} represents the energy of VOC molecules including acetone, benzene, and tetrachloromethane.

RESULTS AND DISCUSSION

We first investigated the adsorption behaviors of acetone, benzene, and tetrachloromethane on pristine BC_6N and observed only a weak interaction between the VOCs and the monolayer. To enhance the adsorption, the Pd atom was introduced into the BC_6N monolayer through interstitial doping. Then, the adsorption performance of the Pd-doped BC_6N monolayer toward three VOC molecules was examined. The adsorption distance, adsorption energy, charge transfer, and band structure were calculated and compared in order to find the most suitable adsorbate−adsorbent systems.

Molecules and Monolayers. *VOC Molecules.* Calculations for VOC molecules were performed with the converged values of the plane-wave kinetic energy cutoff and cell size. Specifically, the energy cutoffs for acetone, benzene, and tetrachloromethane are 22, 25, and 22 Ha, respectively. To mitigate any cell size effects, a supercell of 18 × 18 × 18 $Bohr^3$ is employed for all three VOC molecules. With these converged parameters, the atomic structures of the three VOC molecules are optimized. In acetone, the bond lengths for C−H, C−C, and C−O are 1.10, 1.51, and 1.22 Å, respectively. Bond angles are also determined, measuring 106.5, 110.9, 116.6, and 121.7° for H−C−H, H−C−C, C−C−C, and C−C−O angles, respectively. Benzene has a hexagonal carbon ring structure featuring bond angles of 120.0° for H−C−C and C−C−C. The bond lengths for C−H and C−C are 1.09 and 1.40 Å, respectively. Tetrachloromethane shows a tetrahedral structure with a central C atom and four chlorine (Cl) atoms at the vertices. The C−Cl bond length and Cl−C−Cl bond angle are calculated to be 1.78 Å and 109.5°, respectively. The above results are in excellent agreement with

https://doi.org/10.1021/acsomega.3c06325
ACS Omega 2023, 8, 46841−46850

Table 3. Optimized Structural Parameters of the Pristine and Pd-Doped BC_6N Monolayers: Lattice Constant (a) in Å, Bond Lengths (d) of C−B, C−C, C−N, Pd−B, and Pd−C in Å, Defect Formation Energy (E_{form}) in eV, and Energy Band Gap (E_g) in eV

structure	A	d_{CB}	d_{CC}	d_{CN}	d_{Pd-B}	d_{Pd-C}	E_{form}	E_g
pristine BC_6N	4.977	1.47	1.41	1.45				1.273
Pd-doped BC_6N	4.982	1.48	1.43	1.45	2.24	2.13	2.277	1.075

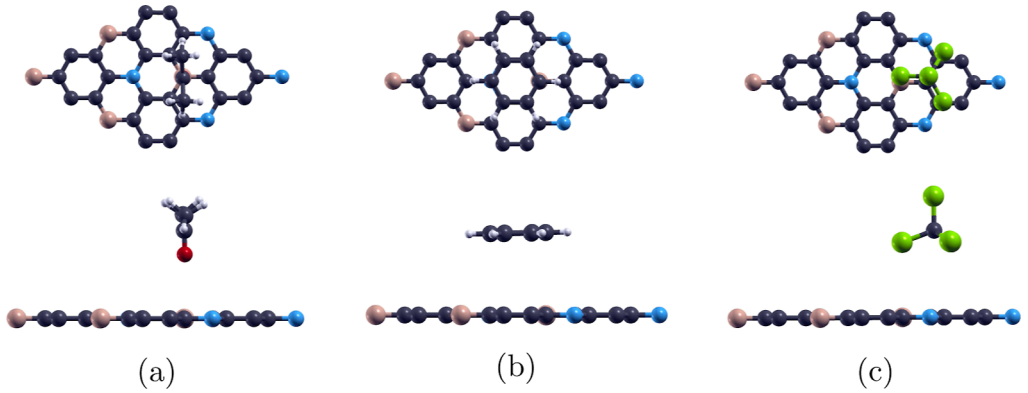

Figure 4. Top and side views of the optimized configurations for VOCs adsorbed on the pristine 2 × 2 BC_6N monolayer. (a) Acetone on BC_6N. (b) Benzene on BC_6N. (c) Tetrachloromethane on BC_6N. H, B, C, N, O, and Cl atoms are represented by white, pink, gray, blue, red, and green, respectively.

experimental data,[53] and a detailed comparison can be seen in Table 2.

Pristine 2 × 2 BC_6N Monolayer. To better understand the structural properties of the pristine BC_6N monolayer, we performed convergence calculations. The energy cutoff value and vacuum height reach convergence at 25 Ha and 15 Bohr, respectively. The *k*-point mesh is converged at 6 × 6 × 1 for 1 × 1 BC_6N, and the value is changed to 4 × 4 × 1 for calculations containing 2 × 2 BC_6N supercells. As presented in Figure 3a, the optimized 2 × 2 BC_6N monolayer has a graphene-like hexagonal lattice, showing an sp^2 hybridized trigonal planar geometry. There are eight atoms (1 B atom, 1 N atom, and 6 C atoms) per unit cell, with the lattice constant calculated to be 4.977 Å. The C−B, C−C, and C−N bond lengths are 1.47, 1.41, and 1.45 Å, respectively. The bond angles of C−B−C, C−C−C, and C−N−C are 120.0, 121.3, and 120.0°, respectively. Based on band structure calculation, BC_6N is a direct semiconductor with an energy band gap of 1.273 eV, as presented in Figure 3b and Table 3. The above results are in accordance with previous literature studies, which suggest a lattice constant of 4.99 Å, a band gap of 1.28 eV, and bond lengths of 1.47, 1.42, and 1.45 Å for C−B, C−C, and C−N, respectively.[43,44,54]

Pd-Doped BC_6N Monolayer. The Pd-doped BC_6N monolayer was formed by introducing an interstitial transition metal dopant into the pristine 2 × 2 BC_6N. As the converged value of the plane-wave kinetic energy cutoff for the Pd crystal lattice (20 Ha) is smaller than the energy cutoff for the pristine BC_6N monolayer, 25 Ha is used in calculations containing the Pd-doped BC_6N monolayer. Further, a *k*-point mesh of ×4 *x* that of the pristine BC_6N monolayer is used to study the doped monolayer, and the converged vacuum height is increased to 20 Bohr.

Using the converged values, a structural optimization calculation was carried out. Based on the result, we determined that the most energy-stable site for Pd doping is above the B−C bond, and the C−Pd−B angle is 39.6°, as shown in Figure 3a. The doping site is slightly different from the position suggested by previous research, in which Pd is 2.13 Å above the C atom of BC_6N.[43] In the force-relaxed structure of the Pd-doped BC_6N monolayer, the atomic distances of Pd−B and Pd−C are 2.24 and 2.13 Å, respectively. As the Pd−B and Pd−C distances are smaller than the Pd−B radii sums of 2.56 Å and the Pd−C radii sums of 2.34 Å, a chemical bond is formed between Pd−B and Pd−C. Upon the interaction with Pd, the bond lengths of C−B and C−C near the doping site are also elongated from 1.47 and 1.41 Å to 1.48 and 1.43 Å, respectively. The lattice constant for Pd-doped BC_6N is 4.982 Å, showing a small increase from the 4.977 Å lattice constant for pristine 2 × 2 BC_6N, as illustrated in Table 3. Based on eq 3, the defect formation energy for the Pd-doped BC_6N monolayer is calculated to be 2.277 eV, indicating its energy-consuming formation process.

Through modifying the atomic arrangement, the Pd dopant also induces changes in the electronic properties of the BC_6N monolayer. As a transition metal impurity, Pd introduces additional electronic states and creates a local strain field in the lattice of BC_6N. This interplay between the dopant atom and the host material changes the electronic structure and tunes the band gap. It can be seen in the band structure plot in Figure 3b that after Pd doping, the band gap of BC_6N is narrowed, from 1.273 to 1.075 eV. The obtained value is consistent with the previous result, which suggests a band gap of 1.080 eV for Pd-doped BC_6N.[43] With the altered band gap and more desirable physical characteristics, Pd-doped BC_6N offers great potential in a range of optoelectronic devices.

VOC Adsorption on Pristine BC_6N. The adsorption behaviors of VOC molecules on the pristine BC_6N monolayer were then analyzed. To ensure the accuracy of our results, the vacuum heights were calculated, converging at 26, 19, and 27 Bohr for acetone, benzene, and tetrachloromethane on BC_6N, respectively. After the initial placements, all VOCs−BC_6N adsorption complexes were optimized to the most energetically stable configurations. As illustrated in Figure 4, acetone

https://doi.org/10.1021/acsomega.3c06325
ACS Omega 2023, 8, 46841−46850

assumes a vertical configuration with its oxygen (O) atom directed toward the B atom of BC_6N. The minimum adsorption distance, measured between the O and B atoms, is 3.30 Å. When benzene interacts with BC_6N, it is slightly tilted upward but still maintains a parallel orientation. The hexagonal arrangement of carbon atoms in benzene aligns with the B−C−N hexagon of BC_6N, resulting in an adsorption distance of 4.12 Å. In the case of tetrachloromethane adsorption, the molecule orients itself with the three Cl atoms facing the BC_6N monolayer. The two Cl atoms positioned above the C atoms are slightly elevated compared with the Cl atom above the B atom. This can be explained by the stronger attractive force between the Cl and B atoms. The shortest adsorption distance, or the Cl−B distance, is measured to be 3.93 Å.

The atomic radii of B, C, O, and Cl atoms are 0.87, 0.67, 0.48, and 0.79 Å, respectively. The minimum adsorption distances for acetone, benzene, and tetrachloromethane on the BC_6N monolayer are found to be 3.30, 4.12, and 3.93 Å, respectively. The corresponding atomic radii sums are 1.35 Å for O−B, 1.34 Å for C−C, and 1.66 Å for Cl−B. As the minimum distances between the VOCs and the BC_6N monolayer are greater than the atomic radii sums of O−B, C−C, and Cl−B, the three gas molecules are physically adsorbed only on pristine BC_6N.

Using eq 4, the adsorption energies of VOCs on a pristine BC_6N monolayer were calculated, as displayed in Table 4. The adsorption energies for acetone, benzene, and tetrachloromethane are −0.003, −0.036, and −0.017 eV (1 eV equals 0.0367 Hartree), respectively. The negative energy indicates an exothermic and spontaneous adsorption process, but the small absolute value suggests that the adsorption of gas molecules involves only weak physisorption.

Table 4. Adsorption Energy (E_{ad}), Minimum Adsorption Distance (d), Energy Band Gap (E_g), and Percent Change in the Band Gap (% ΔE_g) for VOC Adsorption on Pristine and Pd-Doped BC_6N Monolayers[a]

system	E_{ad} (eV)	d (Å)	E_g (eV)	% ΔE_g (%)
pBC_6N			1.273	
$pBC_6N-C_3H_6O$	−0.003	3.30 (O−B)	1.274	0.08
$pBC_6N-C_6H_6$	−0.036	4.12 (C−C)	1.272	−0.08
pBC_6N-CCl_4	−0.017	3.93 (Cl−B)	1.271	−0.15
$PdBC_6N$			1.075	
$PdBC_6N-C_3H_6O$	−0.745	2.08 (Pd−O)	1.123	4.47
$PdBC_6N-C_6H_6$	−1.028	2.17 (Pd−C)	1.100	2.33

[a] pBC_6N and $PdBC_6N$ are pristine and Pd-doped BC_6N monolayers, respectively. Acetone, benzene, and tetrachloromethane are represented by their chemical formulas C_3H_6O, C_6H_6, and CCl_4, respectively.

The small adsorption energies of VOCs on pristine BC_6N correspond to the minimal charge transfer in the VOCs-adsorbed BC_6N systems. As visualized in Figure 5, the red region indicates electron accumulation, and the blue region signifies electron depletion. It can be seen that upon VOC adsorption, BC_6N tends to act as an electron donor, showing charge depletion. In the case of acetone adsorption, the higher electronegativity of the O atom induces a negative charge density around the B atom. When adsorbed with benzene, BC_6N shows electron depletion at the B−C−N hexagon. For tetrachloromethane, the electron acceptor behavior of its Cl atoms depletes the electron charge around the B and C atoms in BC_6N. The absence of an overlap between the red and blue regions implies that little electron transfer is occurring in the VOCs−BC_6N systems, suggesting weak adsorption.

To explore potential changes in the electronic structure of BC_6N induced by VOC adsorption, we conducted band structure calculations, and the results are presented in Figure 6. Upon comparison with the band structure of pristine BC_6N in Figure 6, it is evident that VOC adsorption exerts a minimal influence on the electronic band arrangement near the Fermi level. Consistent with this observation, the calculated band gaps exhibit marginal shifts, transitioning from 1.273 eV in pristine BC_6N to 1.274, 1.272, and 1.271 eV following the adsorption of acetone, benzene, and tetrachloromethane, respectively. While acetone leads to a band gap increase of 0.08%, benzene and tetrachloromethane experience 0.08 and 0.15% narrowing of the band gap, respectively. These slight variations in the band gap further confirm the weak interaction between the VOCs and the pristine monolayer.

VOC Adsorption on Pd-Doped BC_6N. Pd, a transition metal, was interstitially doped into the BC_6N monolayer to improve the adsorption performance, as illustrated in Figure 3.

To investigate the adsorption behaviors of acetone, benzene, and tetrachloromethane on a Pd-doped BC_6N monolayer, we extended the vacuum heights to 32, 28, and 33 Bohr, respectively. Acetone was initially placed with its O atom positioned above the Pd dopant, while benzene had its C−C bond situated on the top of the Pd atom. Tetrachloromethane was inversely positioned with its Cl atom oriented toward the Pd atom. Following structural optimization, it was observed that both acetone and benzene were effectively adsorbed onto the Pd-doped BC_6N monolayer with the same configurations on pristine BC_6N. However, tetrachloromethane failed to maintain a stable structure upon adsorption on Pd-doped BC_6N. The strong force between the Cl atom and Pd atom

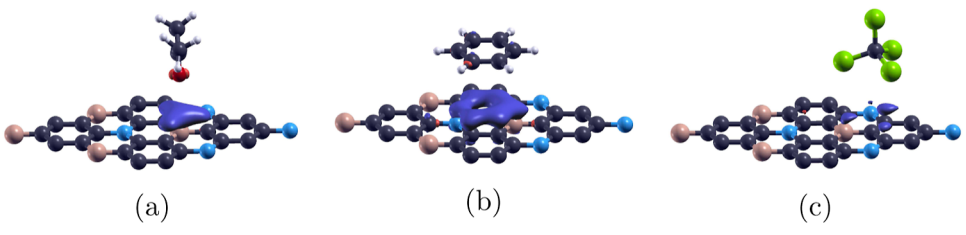

Figure 5. Charge transfer of VOCs on the pristine 2 × 2 BC_6N monolayer. (a) Acetone−BC_6N system. (b) Benzene−BC_6N system. (c) Tetrachloromethane−BC_6N system. H, B, C, N, O, and Cl atoms are represented by white, pink, gray, blue, red, and green, respectively. The red and blue loops indicate electron accumulation and electron depletion, respectively. The isovalues are set to be 0.003, 0.001, and 0.001 e/Å^3 for acetone, benzene, and tetrachloromethane on BC_6N, respectively.

https://doi.org/10.1021/acsomega.3c06325
ACS Omega 2023, 8, 46841−46850

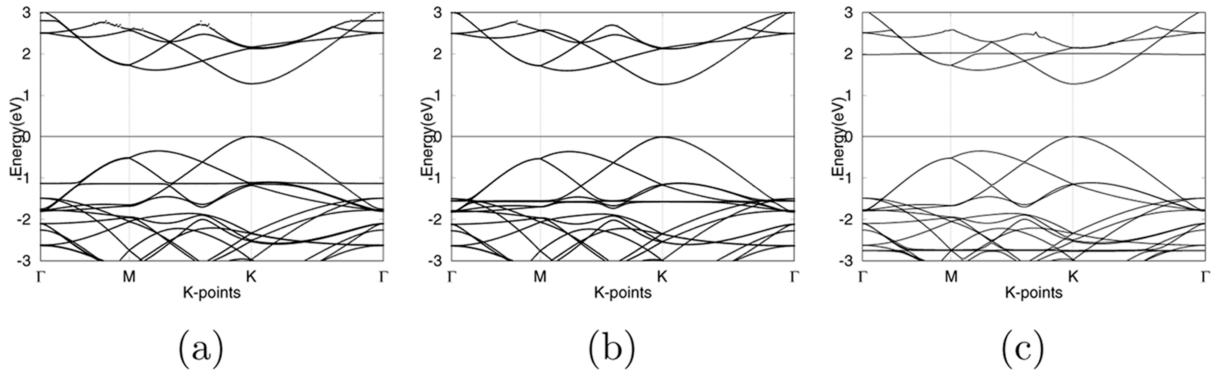

Figure 6. Electronic band structures of the pristine 2 × 2 BC_6N monolayer with VOCs adsorbed. (a) Acetone−BC_6N complex. (b) Benzene−BC_6N complex. (c) Tetrachloromethane−BC_6N complex. The Fermi level is set at zero, and the conduction band minimum (CBM) and the valence band maximum (VBM) are located at the *K* point.

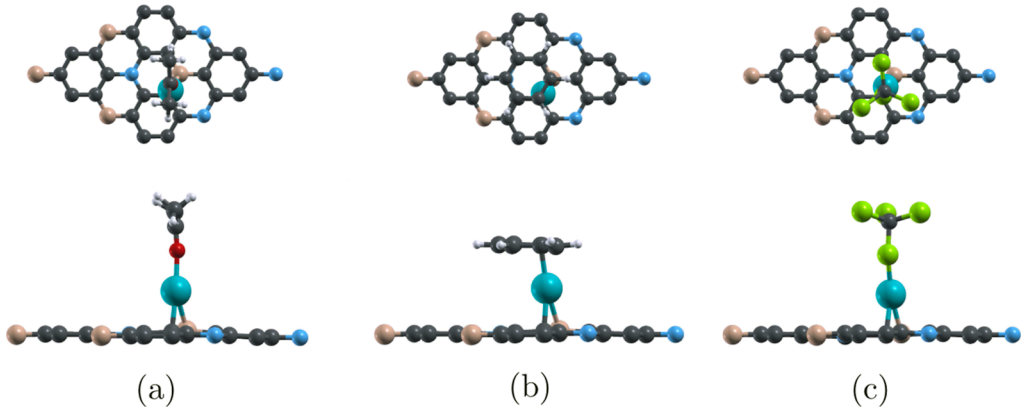

Figure 7. Top and side views of VOCs adsorbed on the Pd-doped BC_6N monolayer: (a) optimized configuration for acetone adsorption, (b) optimized configuration for benzene adsorption, and (c) initial configuration for tetrachloromethane adsorption. H, B, C, N, O, Cl, and Pd atoms are represented by white, pink, gray, blue, red, green, and cyan, respectively.

resulted in the breakage of the C−Cl bond of tetrachloromethane, leading to the formation of an unstable and unadsorbed CCl_3^+ species. As presented in Figure 7, acetone adopts a slightly tilted vertical orientation when adsorbed on Pd-doped BC_6N, making an angle of 170.4° with the Pd atom (C−O−Pd). The O atom of acetone is chemically bonded to Pd with a bond length of 2.08 Å. Due to the interaction between the O atom and Pd atom, both the C−O bond of acetone and the Pd−B bond of BC_6N experience slight elongations from 1.22 and 2.24 Å to 1.23 and 2.27 Å, respectively, while the Pd−C bond of BC_6N exhibits a minor shortening from 2.13 to 2.11 Å. Benzene prefers a parallel orientation, with its C−C bond above the Pd atom. This configuration leads to the formation of a Pd−C bond with a length of 2.17 Å, resulting in an increase of the C−C bond of benzene from 1.40 to 1.42 Å. Furthermore, both the Pd−B and Pd−C bonds of BC_6N experience elongations to 2.36 and 2.15 Å, respectively. Notably, the bond length of Pd−B shows a 5% increase, indicating a significant attraction between the Pd atom of BC_6N and the C atom of benzene.

The enhanced adsorption performance of the BC_6N monolayer is further corroborated by the increased values of adsorption energy. Because of the formation of chemical bonds between Pd and the gas molecules, the adsorption energies of acetone and benzene on Pd-doped BC_6N become more negative, changing to −0.745 and −1.028 eV, respectively. Pd-doped BC_6N shows better adsorption performance than most other 2D monolayers, including stanene, single-vacancy silicene, black phosphorus, and GeS.[55−58] Additionally, the strong adsorption energies of acetone and benzene on Pd-doped BC_6N are also comparable to those observed on the Al-doped C_2N monolayer and transition-metal-deposited single-vacancy defective graphene.[59,60]

Charge transfer calculations were then conducted to analyze the adsorption behavior of acetone and benzene on Pd-doped BC_6N. As depicted in Figure 8, a notable overlap of the red and blue regions is observed, signifying the exchange of electrons and the formation of chemical bonds between the VOC molecules and the Pd-doped BC_6N monolayer. Due to the higher electronegativity of the O atom in acetone and the C atom in benzene, there is electron accumulation in these regions, while charge depletion occurs around the Pd atom in BC_6N. This observation of chemisorption aligns with the greatly enhanced adsorption energies and reduced adsorption distances, further underscoring the improved adsorption mechanism after doping.

The electronic properties of the Pd-doped BC_6N monolayer were further analyzed with the VOCs adsorbed. The band structures for the acetone−BC_6N and benzene−BC_6N complexes are illustrated in Figure 8. It can be seen that there is a modification in the direct band gap of Pd-doped BC_6N from 1.075 to 1.123 and 1.100 eV after acetone and benzene adsorption, respectively. This corresponds to the percent changes in the band gap of 4.47 and 2.33%,

https://doi.org/10.1021/acsomega.3c06325
ACS Omega 2023, 8, 46841−46850

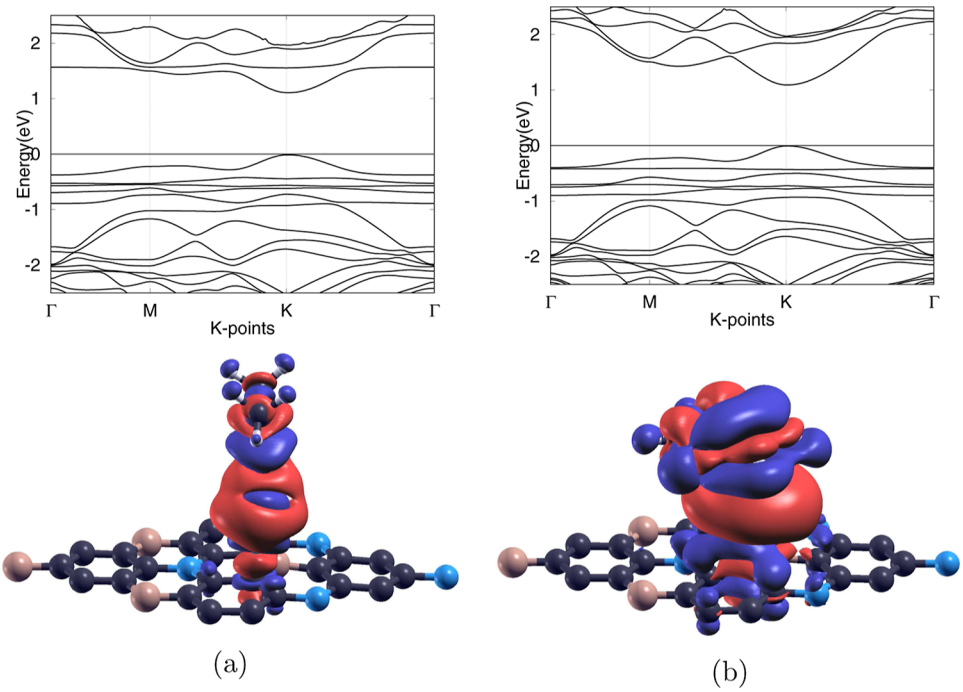

Figure 8. Electronic band structures (first row) and charge transfer (second row) of VOCs adsorbed on a Pd-doped BC_6N monolayer. For the band structure plot, the Fermi level is set at zero, and the conduction band minimum (CBM) and the valence band maximum (VBM) are located at the *K* point. In the charge transfer plot, H, B, C, N, O, and Pd atoms are represented by white, pink, gray, blue, red, and cyan, respectively. The red and blue loops indicate electron accumulation and electron depletion, respectively. The isovalues are set to be 0.003 and 0.001 e/Å^3 for acetone and benzene on Pd-doped BC_6N, respectively. (a) Acetone adsorbed on Pd-doped BC_6N. (b) Benzene adsorbed on Pd-doped BC_6N.

respectively, as outlined in Table 4. Accordingly, in comparison to pristine BC_6N, Pd-doped BC_6N exhibits a more pronounced alteration in its band structure after the adsorption of acetone and benzene. This can be attributed to the heightened interaction between the gas molecules and the monolayer.

As suggested by the above findings, interstitially doping the Pd atom is an effective method to enhance the adsorption behavior of BC_6N toward VOCs. This can be attributed to the doping-induced structural change in BC_6N. When incorporated into the BC_6N semiconductor lattice, Pd introduces additional charge carriers and creates favorable sites for interactions with VOC molecules. Moreover, the electronic configuration of Pd facilitates a stronger affinity for electron exchange with the adsorbates, increasing the charge transfer in the VOC-adsorbed BC_6N systems. This, in turn, reduces the distance between the adsorbent and the VOC molecules, leading to stronger and more stable chemisorption. The result is an increase in adsorption energy values, as observed in our study. Altogether, Pd doping offers electronic and structural alterations that substantially enhance the adsorption capability of BC_6N toward acetone and benzene. With its superior adsorption performance, Pd-doped BC_6N holds great potential in mitigating air pollution and improving public health conditions.

CONCLUSIONS

Here, we carried out first-principles calculations based on DFT to explore the adsorption behaviors of three representative toxic VOC gases (acetone, benzene, and tetrachloromethane) on pristine and Pd-doped BC_6N monolayers. The obtained results disclosed that the interaction between VOCs and pristine BC_6N was governed by weak physisorption, which may limit its use in gas adsorption devices. To enhance its adsorption capacity, we adopted the technique of doping impurities and introduced a transitional metal Pd into the BC_6N monolayer. Because of the modification in the electronic structure of BC_6N, acetone and benzene were adsorbed with energies of −0.745 and −1.028 eV, showing 248.3 and 28.6 times increases in values compared to those of the pristine BC_6N monolayer, respectively. The overlap of charge accumulation and charge depletion suggested the occurrence of chemisorption, indicating successful capture of VOCs by the adsorbent. Based on the above findings, a Pd-doped BC_6N monolayer was proposed as a promising material for ambient VOC removal, and the potential of tailoring BC_6N-based materials for more efficient VOC control was also highlighted. Therefore, we encourage future research to investigate other environmentally friendly applications of BC_6N such as photocatalysts. It is also recommended that we dope other elements in BC_6N to develop higher-performance adsorbents and explore ways to recycle the used adsorbents.

AUTHOR INFORMATION

Corresponding Author

Xuan Luo − *National Graphene Research and Development Center, Springfield, Virginia 22151, United States;* orcid.org/0000-0002-0592-0610; Email: xluo@ngrd.org

Author

Xiaoshu Jiang − *National Graphene Research and Development Center, Springfield, Virginia 22151, United States;* orcid.org/0009-0009-9698-5134

Complete contact information is available at: https://pubs.acs.org/10.1021/acsomega.3c06325

https://doi.org/10.1021/acsomega.3c06325
ACS Omega 2023, 8, 46841−46850

Notes

The authors declare no competing financial interest.

■ ACKNOWLEDGMENTS

We would like to thank Dr. Gefei Qian for the valuable technical support he provided. This research received no external funding.

■ REFERENCES

(1) Oseh, C. How mobile clinics are helping those affected by Canada's wildfires. *Br. Med. J.* **2023**, *382*, 2007.
(2) Coogan, S. C.; Daniels, L. D.; Boychuk, D.; Burton, P. J.; Flannigan, M. D.; Gauthier, S.; Kafka, V.; Park, J. S.; Wotton, B. M. Fifty years of wildland fire science in Canada. *Can. J. For. Res.* **2021**, *51*, 283−302.
(3) Tymstra, C.; Stocks, B. J.; Cai, X.; Flannigan, M. D. Wildfire management in Canada: Review, challenges and opportunities. *Prog. Disaster Sci.* **2020**, *5*, 100045.
(4) McGee, T.; McFarlane, B.; Tymstra, C. *Wildfire hazards, risks and disasters*; Elsevier, 2015, pp 35−58.
(5) Landrigan, P. J. Air pollution and health. *Lancet Public Health* **2017**, *2*, e4−e5.
(6) Manisalidis, I.; Stavropoulou, E.; Stavropoulos, A.; Bezirtzoglou, E. Environmental and health impacts of air pollution: a review. *Front. Public Health* **2020**, *8*, 14.
(7) Kampa, M.; Castanas, E. Human health effects of air pollution. *Environ. Pollut.* **2008**, *151*, 362−367.
(8) Oesch, S.; Faller, M. Environmental effects on materials: The effect of the air pollutants SO2, NO2, NO and O3 on the corrosion of copper, zinc and aluminium. A short literature survey and results of laboratory exposures. *Corros. Sci.* **1997**, *39*, 1505−1530.
(9) Rani, B.; Singh, U.; Chuhan, A.; Sharma, D.; Maheshwari, R. Photochemical smog pollution and its mitigation measures. *J. Adv. Sci. Res.* **2011**, *2*, 28−33.
(10) Mozaffar, A.; Zhang, Y.-L. Atmospheric volatile organic compounds (VOCs) in China: a review. *Curr. Pollut. Rep.* **2020**, *6*, 250−263.
(11) Niu, Y.; Yan, Y.; Chai, J.; Zhang, X.; Xu, Y.; Duan, X.; Wu, J.; Peng, L. Effects of regional transport from different potential pollution areas on volatile organic compounds (VOCs) in Northern Beijing during non-heating and heating periods. *Sci. Total Environ.* **2022**, *836*, 155465.
(12) Yang, C.; Miao, G.; Pi, Y.; Xia, Q.; Wu, J.; Li, Z.; Xiao, J. Abatement of various types of VOCs by adsorption/catalytic oxidation: A review. *Chem. Eng. J.* **2019**, *370*, 1128−1153.
(13) Zhang, X.; Gao, B.; Creamer, A. E.; Cao, C.; Li, Y. Adsorption of VOCs onto engineered carbon materials: A review. *J. Hazard Mater.* **2017**, *338*, 102−123.
(14) Kamal, M. S.; Razzak, S. A.; Hossain, M. M. Catalytic oxidation of volatile organic compounds (VOCs)−A review. *Atmos. Environ.* **2016**, *140*, 117−134.
(15) Li, X.; Zhang, L.; Yang, Z.; Wang, P.; Yan, Y.; Ran, J. Adsorption materials for volatile organic compounds (VOCs) and the key factors for VOCs adsorption process: A review. *Sep. Purif. Technol.* **2020**, *235*, 116213.
(16) Soni, V.; Singh, P.; Shree, V.; Goel, V. Effects of VOCs on human health. *Air Pollut. Control* **2018**, 119−142.
(17) David, E.; Niculescu, V.-C. Volatile organic compounds (VOCs) as environmental pollutants: Occurrence and mitigation using nanomaterials. *Int. J. Environ. Res. Publ. Health* **2021**, *18*, 13147.
(18) Zhang, L.; Wang, B.; Li, K.; Wang, Z.; Xu, D.; Su, Y.; Wu, D.; Xie, B. Non-negligible health risks caused by inhalation exposure to aldehydes and ketones during food waste treatments in megacity Shanghai. *Environ. Pollut.* **2023**, *325*, 121448.
(19) Mirzaei, A.; Leonardi, S.; Neri, G. Detection of hazardous volatile organic compounds (VOCs) by metal oxide nanostructures-based gas sensors: A review. *Ceram. Int.* **2016**, *42*, 15119−15141.
(20) Huang, B.; Lei, C.; Wei, C.; Zeng, G. Chlorinated volatile organic compounds (Cl-VOCs) in environment—sources, potential human health impacts, and current remediation technologies. *Environ. Int.* **2014**, *71*, 118−138.
(21) Kim, S. C.; Shim, W. G. Catalytic combustion of VOCs over a series of manganese oxide catalysts. *Appl. Catal. B Environ.* **2010**, *98*, 180−185.
(22) Parmar, G. R.; Rao, N. Emerging control technologies for volatile organic compounds. *Crit. Rev. Environ. Sci. Technol.* **2008**, *39*, 41−78.
(23) Adelodun, A. A. Influence of operation conditions on the performance of non-thermal plasma technology for VOC pollution control. *J. Ind. Eng. Chem.* **2020**, *92*, 41−55.
(24) Dwivedi, P.; Gaur, V.; Sharma, A.; Verma, N. Comparative study of removal of volatile organic compounds by cryogenic condensation and adsorption by activated carbon fiber. *Sep. Purif. Technol.* **2004**, *39*, 23−37.
(25) Jeong, G. H.; Sasikala, S. P.; Yun, T.; Lee, G. Y.; Lee, W. J.; Kim, S. O. Nanoscale assembly of 2D materials for energy and environmental applications. *Adv. Mater.* **2020**, *32*, 1907006.
(26) Cao, J.; Wu, F.; Wen, M.; Peng, J.; Yang, Y.; Dong, H. Adsorption mechanism of typical VOCs on pristine and Al-modified MnO2 monolayer. *Appl. Surf. Sci.* **2021**, *539*, 148164.
(27) Yadav, A. Monolayer Silicon Carbide as an Efficient Adsorbent for Volatile Organic Compounds: An Ab Initio Approach. *Silicon* **2022**, *15*, 1563−1569.
(28) Kadhim, M. M.; Hadi, M. A.; Hachim, S. K.; Abed, Z. T.; Abdullaha, S. A.; Rheima, A. M. Quantum Chemical Study the Removal of Acetone by Using the Pristine and Si-doped C2N Monolayer. *Silicon* **2023**, *15*, 5105.
(29) Ganji, M. D.; Mazaheri, H.; Khosravi, A. Acetone adsorption on pristine and Pt-doped graphene: a first-principles vdW-DF study. *Commun. Theor. Phys.* **2015**, *64*, 576−582.
(30) Qu, Y.; Ding, J.; Chen, H.; Peng, J. Effect of noble metal atoms on adsorption and electronic properties of graphene toward toxic gas. *Comput. Theor. Chem.* **2021**, *1196*, 113115.
(31) Tang, X.; Du, A.; Kou, L. Gas sensing and capturing based on two-dimensional layered materials: Overview from theoretical perspective. *Wiley Interdiscip. Rev.: Comput. Mol. Sci.* **2018**, *8*, No. e1361.
(32) Bagherzadeh, M.; Farahbakhsh, A. Surface functionalization of graphene. *Graphene Mater. Fund. Emerg. App.* **2015**, 25−65.
(33) Agnoli, S.; Favaro, M. Doping graphene with boron: a review of synthesis methods, physicochemical characterization, and emerging applications. *J. Mater. Chem. A* **2016**, *4*, 5002−5025.
(34) Yang, S.; Li, W.; Ye, C.; Wang, G.; Tian, H.; Zhu, C.; He, P.; Ding, G.; Xie, X.; Liu, Y.; et al. C3N—A 2D crystalline, hole-free, tunable-narrow-bandgap semiconductor with ferromagnetic properties. *Adv. Mater.* **2017**, *29*, 1605625.
(35) Mehdi Aghaei, S.; Monshi, M.; Torres, I.; Zeidi, S.; Calizo, I. DFT study of adsorption behavior of NO, CO, NO2, and NH3 molecules on graphene-like BC3: a search for highly sensitive molecular sensor. *Appl. Surf. Sci.* **2018**, *427*, 326−333.
(36) Zhao, Z.; Yong, Y.; Gao, R.; Hu, S.; Zhou, Q.; Su, X.; Kuang, Y.; Li, X. Adsorption, sensing and optical properties of molecules on BC3 monolayer: First-principles calculations. *Mater. Sci. Eng. B* **2021**, *271*, 115266.
(37) Bafekry, A.; Ghergherehchi, M.; Farjami Shayesteh, S.; Peeters, F. Adsorption of molecules on C3N nanosheet: A first-principles calculations. *Chem. Phys.* **2019**, *526*, 110442.
(38) Pashangpour, M.; Peyghan, A. A. Adsorption of carbon monoxide on the pristine, B-and Al-doped C 3 N nanosheets. *J. Mol. Model.* **2015**, *21*, 116−117.
(39) Matsui, K.; Oda, S.; Yoshiura, K.; Nakajima, K.; Yasuda, N.; Hatakeyama, T. One-shot multiple borylation toward BN-doped nanographenes. *J. Am. Chem. Soc.* **2018**, *140*, 1195−1198.
(40) Mortazavi, B. Ultrahigh thermal conductivity and strength in direct-gap semiconducting graphene-like BC6N: A first-principles and classical investigation. *Carbon* **2021**, *182*, 373−383.

https://doi.org/10.1021/acsomega.3c06325
ACS Omega 2023, 8, 46841−46850

(41) Abdullah, N. R.; Abdullah, B. J.; Tang, C.-S.; Gudmundsson, V. Properties of BC6N monolayer derived by first-principle computation: Influences of interactions between dopant atoms on thermoelectric and optical properties. *Mater. Sci. Semicond. Process.* **2021**, *135*, 106073.
(42) Yong, Y.; Ren, F.; Zhao, Z.; Gao, R.; Hu, S.; Zhou, Q.; Kuang, Y. Highly enhanced NH3-sensing performance of BC6N monolayer with single vacancy and Stone-Wales defects: A DFT study. *Appl. Surf. Sci.* **2021**, *551*, 149383.
(43) Aasi, A.; Mehdi Aghaei, S.; Panchapakesan, B. Outstanding performance of transition-metal-decorated single-layer graphene-like BC6N nanosheets for disease biomarker detection in human breath. *ACS Omega* **2021**, *6*, 4696−4707.
(44) Aghaei, S.; Aasi, A.; Farhangdoust, S.; Panchapakesan, B. Graphene-like BC6N nanosheets are potential candidates for detection of volatile organic compounds (VOCs) in human breath: A DFT study. *Appl. Surf. Sci.* **2021**, *536*, 147756.
(45) Perdew, J. P.; Burke, K.; Ernzerhof, M. Generalized gradient approximation made simple. *Phys. Rev. Lett.* **1996**, *77*, 3865−3868.
(46) Gonze, X.; Amadon, B.; Anglade, P.-M.; Beuken, J.-M.; Bottin, F.; Boulanger, P.; Bruneval, F.; Caliste, D.; Caracas, R.; Côté, M.; et al. ABINIT: First-principles approach to material and nanosystem properties. *Comput. Phys. Commun.* **2009**, *180*, 2582−2615.
(47) Blöchl, P. E. Projector augmented-wave method. *Phys. Rev. B* **1994**, *50*, 17953−17979.
(48) Holzwarth, N.; Tackett, A.; Matthews, G. A Projector Augmented Wave (PAW) code for electronic structure calculations, Part I: atompaw for generating atom-centered functions. *Comput. Phys. Commun.* **2001**, *135*, 329−347.
(49) Basiuk, V. A.; Prezhdo, O. V.; Basiuk, E. V. Thermal smearing in DFT calculations: How small is really small? A case of La and Lu atoms adsorbed on graphene. *Mater. Today Commun.* **2020**, *25*, 101595.
(50) Hwang, Y.-H.; Lee, Y.-K. Structure and activity of unsupported NiWS2 catalysts for slurry phase hydrocracking of vacuum residue: XAFS studies. *J. Catal.* **2021**, *403*, 131−140.
(51) Martínez-Flores, C.; Bolívar-Pineda, L. M.; Basiuk, V. A. Lanthanide bisphthalocyanine single-molecule magnets: A DFT survey of their geometries and electronic properties from lanthanum to lutetium. *Mater. Chem. Phys.* **2022**, *287*, 126271.
(52) Head, J. D.; Zerner, M. C. A Broyden—Fletcher—Goldfarb—Shanno optimization procedure for molecular geometries. *Chem. Phys. Lett.* **1985**, *122*, 264−270.
(53) Kuchitsu, K. *Structure of free polyatomic molecules: basic data*; Springer Science & Business Media, 2013.
(54) Mortazavi, B.; Shahrokhi, M.; Raeisi, M.; Zhuang, X.; Pereira, L. F. C.; Rabczuk, T. Outstanding strength, optical characteristics and thermal conductivity of graphene-like BC3 and BC6N semiconductors. *Carbon* **2019**, *149*, 733−742.
(55) Vo, V. O.; Pham, T. L.; Dinh, V. A. Adsorption of acetone and toluene on single-vacancy silicene by density functional theory calculations. *Mater. Trans.* **2020**, *61*, 1449−1454.
(56) Li, Y.; Yu, C.-M. DFT study of the adsorption of C6H6 and C6H5OH molecules on stanene nanosheets: Applications to sensor devices. *Phys. E Low-dimens. Syst. Nanostruct.* **2021**, *127*, 114533.
(57) Ou, P.; Song, P.; Liu, X.; Song, J. Superior sensing properties of black phosphorus as gas sensors: a case study on the volatile organic compounds. *Adv. Theor. Simulat.* **2019**, *2*, 1800103.
(58) Pu, K.; Dai, X.; Bu, Y.; Guo, R.; Tao, W.; Jia, D.; Song, J.; Zhao, T.; Feng, L. Al-doped GeS nanosheet as a promising sensing material for O-contained volatile organic compounds detection. *Appl. Surf. Sci.* **2020**, *527*, 146797.
(59) Su, Y.; Ao, Z.; Ji, Y.; Li, G.; An, T. Adsorption mechanisms of different volatile organic compounds onto pristine C2N and Al-doped C2N monolayer: A DFT investigation. *Appl. Surf. Sci.* **2018**, *450*, 484−491.
(60) Kunaseth, M.; Poldorn, P.; Junkeaw, A.; Meeprasert, J.; Rungnim, C.; Namuangruk, S.; Kungwan, N.; Inntam, C.; Jungsuttiwong, S. A DFT study of volatile organic compounds adsorption on transition metal deposited graphene. *Appl. Surf. Sci.* **2017**, *396*, 1712−1718.

https://doi.org/10.1021/acsomega.3c06325
ACS Omega 2023, 8, 46841−46850